Joint Centre for Mesoscale Meteorology, Reading, UK

Frontal wave stability during moist deformation frontogenesis.

Part 2. The suppression of non-linear wave development.

A. J. Thorpe
C. H. Bishop

Internal Report No. 17

May 1993

Met Office Joint Centre for Mesoscale Meteorology Department of Meteorology
University of Reading PO Box 243 Reading RG6 6BB United Kingdom
Tel: +44 (0)118 931 8425 Fax: +44 (0)118 931 8791
www.metoffice.com

Designed and produced by the Met Office © Crown copyright 2001 01/0240 The Met Office logo is a registered trademark.

Frontal wave stability during moist deformation frontogenesis.

Part 2. The suppression of non-linear wave development.

Craig H. Bishop and Alan J. Thorpe

Department of Meteorology, University of Reading, England.

Abstract.

In this paper, the role of horizontal deformation and the associated frontogenetic ageostrophic circulation in suppressing the development of non-linear waves is assessed. Unless linear barotropic frontal waves can become non-linear, the associated horizontal transports of momentum will not be sufficient to halt frontogenesis or to create non-linear mixing processes such as vortex roll-up. The analysis of Dritschel et al. (1991) suggests that such non-linear phenomena will not occur if the waveslope remains small. Using the linear model described in Part 1, a simple relationship between optimal waveslope amplification over a specified time period and the amplification of an initially isolated edge wave is found. Using this relationship, we investigate how strain affects the dependence of optimal waveslope amplification on wavelength and the time of entry of disturbances to the front. It is found that waves entering the frontal zone when it is intense can experience more steepening than those appearing earlier in the development of the front. The most rapidly growing waves enter the front with a wavelength about three times the width of the front. As the front collapses the ratio of wavelength to frontal width rapidly increases.

For strain rates greater than $0.6\times10^{-5}s^{-1}$, the model predicts that wave slope amplification greater than a factor of e is impossible. More generally, the analysis shows that no amplification is possible for strain rates greater than a quarter of the Coriolis parameter. Thus, our prototype model describes how fronts can achieve structures which would, in the absence of frontogenesis, be highly unstable to along front disturbances.

The variation of optimal growth with wavenumber and the time of entry of disturbances to the front is explained using diagnostics based on a

mathematical model of Bretherton's qualitative description of wave growth in terms of the interaction of counterpropagating edge waves. Notably, these diagnostics yield a prediction for the frontogenesis rate required to *completely* eliminate wave steepening. The technique is relevant to the problem of predicting the minimum attainable cross-frontal scale of a front from the large scale forcing.

1. Introduction

As discussed in Part I of this paper, (Bishop and Thorpe, 1993), horizontal deformation acts to reduce the growth of frontal waves. In this paper, we assess the tendency of such waves to achieve non-linear amplitudes. It is important to assess the likelihood of vortex roll-up not only in the description of the dynamics of the wave but also to investigate whether such processes may prevent frontal collapse to a discontinuity. The dependence of these processes on the deformation rate will be found. For moist fronts, the possibility exists that deformation acts both to increase the potential instability of the front by intensifying the potential vorticity extremum and to suppress waves whilst this intensification occurs. If at a later stage in the frontal development the deformation ceases then the highly unstable structure would be expected to break out in waves. This sequence of events suggests that deformation is crucial in allowing frontal instability to occur but only after deformation has ceased.

The work of Dritschel (1988, Appendix B) and Dritschel et al. (1991) suggests that wave disturbances on vortex strips are unlikely to lead to non-linear processes such as vortex roll up while the wave slope of such disturbances remains small. The major aim of this paper is to determine the frontogenesis rates required to eliminate the possibility of significant frontal wave steepening before a front collapses to a singularity.

The results help in the understanding of whether there is a process, other than viscosity, which limits the horizontal scale of fronts. Using models that implicitly excluded the effects of along front waves and surface friction on frontal collapse, the high resolution numerical studies of Gall (1987) and Garner (1989) were unable to identify any such process.

Along front waves capable of producing down gradient fluxes of heat and momentum might be capable of halting the frontal collapse process. The frontal wave model of Part 1 explicitly represents the linear phase of down gradient horizontal momentum transport produced by barotropic eddies. If these eddies are capable of significantly deforming the front, then non-linear processes such as energy transfers to different wavenumbers or vortex roll-up may prevent the front from collapsing and thus limit the average cross-frontal scale of the front. If, however, the waves remain linear then by definition, they will have a negligible effect on the dynamics of the front and hence its eventual collapse.

Observations such as those of Shapiro et al (1985) demonstrate that frontal widths of the order of a kilometer are possible. Thus, to successfully model the effects of along front waves in such a situation one would have to extend the aforementioned numerical models into a third dimension - a difficult and computationally expensive task. In this respect, the analytic model used in this paper is an ideal prototype model for investigating frontal wave behaviour near the point of frontal collapse.

Dritschel et al (1991), (hereafter DHJS), studied the stability of a barotropic vortex in a linear deformation flow. Whilst this situation is probably relevant to stratospheric flows, tropospheric vortex strips are almost universally *caused* by the ageostrophic response of the atmosphere to the thermal frontogenesis caused by deformation fields. This ageostrophic circulation causes the vorticity of the strip to increase (usually quite rapidly) in time. In DHJS's model the vorticity of the strip remains constant in time. For relatively small and large values of vorticity their vortex strip is stable and unstable, respectively. But as we shall see, it

is misleading to assume that the stability of a vortex strip whose vorticity is changing in time will be a simple average of these two extremes of Dritschel's model. This is because one must take into account the relationship between the width of the strip and its vorticity as governed by Kelvin's circulation theorem. The model to be considered in this work implicitly includes such considerations.

The plan of the paper is as follows. A brief review of the model developed in Part 1 is given in § 2: readers familiar with Part 1 need not read this section. In § 3, we formally define a measure of the non-linear aspect of frontal waves, identify its relationship with wave slope and derive a simple expression for its maximal amplification over a specified time period. The parameter space of maximal amplification is described in § 4. The variation of maximal amplification with wavenumber and on the time of entry of the disturbance onto the strip are described in § 5. This section also contains a diagnostic analysis of these results in terms of a mathematical model of counter propagating edge (Rossby) waves. The edge wave analysis leads to an expression for the maximum instantaneous growth rate of the non-linear aspect of waves and it is used (also in § 5) to predict the strain rate at which increases in wave slope become impossible. In § 6, we discuss the size of the horizontal scales "selected" by the models intensifying PV strip. Section 7 concludes the paper with a discussion of the effects of surface friction on the instability and a calculation of maximal streamfunction growth.

2. Review of analytic model.

The analytic model developed in Part 1 provides a description of frontal wave development on an evolving frontal PV strip. The evolution of this frontal vortex strip is that which would arise from a saturated front

with nearly parallel M and θ_e surfaces, a barotropic low level layer and an along front wind in close geostrophic balance. In order to apply analytic techniques, it was necessary to assume thermal structures yielding discrete regions of uniform low-level vorticity, separated by transition regions. As the analysis in Part I suggested that model cold fronts had very similar stability characteristics to model warm fronts, in this paper we shall only concern ourselves with the occluded front. Furthermore, since the analytic model assumes that interaction between barotropic waves at low levels and those at upper levels are insignificant, we shall only be concerned with regions 2 - 6 of the low-level barotropic layer. Regions 2 and 6 are broad regions of uniform but weak anticyclonic vorticity which surround the uniform strong vorticity of region 4. Regions 3 and 5 are the very narrow transition regions between regions 2 and 4, and 4 and 6, respectively. The front is assumed to lie along the y-axis.

We partition the horizontal wind by writing

$$(u,\ v,\ w) = (-\alpha x + \overline{u}_a + u',\ \alpha y + \overline{v}_g + v',\ \overline{w} + w'). \tag{2.1}$$

The $(-\alpha x,\ \alpha y,\ 0)$ part gives the horizontal deformation wind field. In this paper, we take α to be a constant. The along front geostrophic wind is denoted by $\overline{v}_g$. We use $\overline{v}_{g3}$ and $\overline{v}_{g5}$ to denote the geostrophic wind in the transition regions 3 and 5, respectively. The $(\overline{u}_a,\ \overline{v}_g,\ \overline{w})$ part defines the momentum associated with the developing front. The cross-frontal ageostrophic circulation is described by $\overline{u}_a$ and $\overline{w}$ and we define an ageostrophic streamfunction $\overline{\psi}$ such that $(\overline{u}_a,\ \overline{w}) = (\partial\overline{\psi}/\partial z,\ -\partial\overline{\psi}/\partial x)$. As is evident from eq. (B.1) of Part 1, in the barotropic layer

$$\overline{u}_a = -2\alpha\overline{v}_g/f. \tag{2.2}$$

The symbols u', v' and w' define the flow associated with frontal waves. We assume that the irrotational part of this flow plays only a passive role in

the dynamics and more usually deal only with the non-divergent part of this flow which we denote by $(u'_r, v'_r, 0)$. We express this part of the flow in terms of the perturbation streamfunction Ψ' by setting $(u'_r, v'_r) = (-\partial\Psi'/\partial y, \partial\Psi'/\partial x)$.

Generally, we use the geostrophic coordinates $(X, Y, Z, T) = (x + \bar{v}_g/f, y, z, t)$ and the deforming geostrophic coordinates $(X', Y', Z', T') = (X\exp(\alpha T), Y\exp(-\alpha T), Z, T)$ to describe the system. In terms of the deforming geostrophic coordinates the width of the frontal vortex in region 4 is the constant L, while the width of the transition regions 4 and 6 is the constant δL. The corresponding (time varying) widths in Cartesian space are L_c and δL_c, respectively.

The absolute vorticity in regions 2, 4 and 6 is denoted $\bar{\zeta}_j$ where j = 2, 4 or 6 according to the referenced region and may be written,

$$\bar{\zeta}_j = f\left[1 - E_j\exp(2\alpha T')\right]^{-1}, \qquad (2.3)$$

where f is the Coriolis parameter (here assumed constant) and E_j denotes the constants which relate temperature gradients in deforming geostrophic coordinates to the vorticity of the low-level flow. For the occluded front, $E_2 = E_6 = -0.092$ while $E_4 = 0.5$. Thus, at $T' = 0$ the relative vorticity of the front is assumed to be equal to f; subsequently, it monotonically increases with time until becoming infinite at $T' = t_c$. According to (2.3), $\alpha t_c = 0.347$ or equivalently, $t_c = 9.63\ \text{hr}/(\alpha \times 10^5\ \text{s}^{-1})$. Sometimes it is heuristically useful to describe development in terms of the non-dimensional time T_n, where $T_n = T'/t_c$.

Of particular importance to the stability of the front are the vorticity jumps between regions 2 and 4 and regions 4 and 6. To represent these jumps, we define $\delta\bar{\zeta}_n$ such that, (for the occluded front),

$$\delta\bar{\zeta}_n = \bar{\zeta}_4 - \bar{\zeta}_2 = \bar{\zeta}_4 - \bar{\zeta}_6. \qquad (2.4)$$

Frontal waves are defined entirely in terms of Ψ'. Let Ψ'_2, Ψ'_4 and Ψ'_6 denote Ψ' in regions 2, 4 and 6, respectively. In regions 2 and 6, we take

$$\Psi'_2(x,\ y,\ t) = G(-L_c/2,\ t)\exp\left[il\left(\frac{L_c}{2} + x\right)\right]\exp\left[il\left(y - p'(t)e^{-\alpha t}\right)\right] \qquad (2.5a)$$

$$\Psi'_6(x,\ y,\ t) = G(L_c/2,\ t)\exp\left[il\left(\frac{L_c}{2} - x\right)\right]\exp\left[il\left(y - p'(t)e^{-\alpha t}\right)\right] \qquad (2.5b)$$

where the wavenumber, l, is real and $p'(t)$ is a complex function playing the role of an integrated complex phase speed in deforming coordinates. The $G(x,\ t)$ function, referred to in (2.5a) and (2.5b) defines the horizontal structure of Ψ' in region 4, to be precise,

$$G(x,\ t) = C\ \exp\left(-ilL_c/2\right)\left[lR(t)\sinh\left(lx\right) + \cosh\left(lx\right)\right] \qquad (2.5c)$$

and

$$\Psi'_4(x,\ y,\ t) = G(x,\ t)\ \exp\left[il\left(y - p'(t)e^{-\alpha t}\right)\right]. \qquad (2.5d)$$

In (2.5c), C is a complex constant defining the initial phase and amplitude of the wave, $R(t)$ is a complex function defining the evolution of the horizontal structure of the wave and p' gives the complex phase speed of the wave at $x = 0$. Note that x and t are taken to be non-separable and consequently, in the terminology of Farrell (1984), non-modal solution types are possible.

Note that these forms of Ψ' imply that the perturbation vorticity ζ' $(= \nabla^2\Psi')$ is zero in regions 2, 4 and 6. In the transition regions 3 and 5 the vorticity is non-zero. Because the along front scale of the vorticity perturbations is many orders of magnitude larger than the cross-frontal scale $\zeta' \cong v'_x$ in these regions.

The integral of perturbation vorticity across the transition regions multiplied by $\exp(\alpha T')$, $\tilde{Q}_j$, is of particular dynamical importance. As shown in Part 1, the inviscid vorticity equation requires that

$$\frac{\overline{D}\,\tilde{Q}_j}{D\overline{T}'} + u'_r \, e^{\alpha T'} \delta\overline{\zeta}_n (4 - j) = 0 \qquad (2.6a)$$

$$\frac{\overline{D}}{D\overline{T}'} = \frac{\partial}{\partial \overline{T}'} + \overline{v}_g \frac{\partial}{\partial Y'}, \qquad (2.6b)$$

where in equation form,

$$\tilde{Q}_3 = \left(v'_r(-\frac{L}{2}) - v'_r(-\frac{L}{2} - \delta L)\right)e^{\alpha T'} \text{ and } \tilde{Q}_5 = \left(v'_r(\frac{L}{2} + \delta L) - v'_r(\frac{L}{2})\right)e^{\alpha T'}. \qquad (2.7)$$

The relationship between the $\tilde{Q}_j$ and Ψ' defined in (2.7) implies a very simple relationship between $\tilde{Q}_j$ and the parameters R and p'; *viz.*,

$$\tilde{Q}_3 = Cl_0[lR(T') - 1]\exp\left\{il_0\left[Y' - p'(T')\right]\right\}, \qquad (2.8a)$$

$$\tilde{Q}_5 = Cl_0[-lR(T') - 1]\exp\left\{il_0\left[Y' - p'(T')\right]\right\}. \qquad (2.8b)$$

where $l_0 = l\exp(\alpha T')$. The significance of the R parameter can now be seen. It determines the amplitude ratio of the edge wave in region 3 to that in region 5 and also the phase shift southward, $\Delta\chi$, of the edge wave in region 5 relative to that in region 3, (cf Part 1, § 3).

Using (2.8) and (2.5) in (2.6) yields equations for R and p'; *viz.*,

$$-il_0\left[\left(\frac{dp'}{d\overline{T}'}\right) - \overline{v}_s\right] = R\,\delta\overline{\zeta}_n\left(\frac{l_0\overline{v}_n}{\delta\overline{\zeta}_n} - e^{-\mu}\sinh(\mu)\right) - l\,\delta\overline{\zeta}_s e^{-\mu}\cosh(\mu) \qquad (2.9a)$$

$$\frac{dR}{d\overline{T}'} = -\delta\overline{\zeta}_n\left[R^2\left(\frac{l_0\overline{v}_n}{\delta\overline{\zeta}_n} - e^{-\mu}\sinh(\mu)\right) + \left(\frac{l_0\overline{v}_n}{\delta\overline{\zeta}_n} - e^{-\mu}\cosh(\mu)\right)\right] + lR\,\delta\overline{\zeta}_s e^{-2\mu} \qquad (2.9b)$$

where l_0 is a constant such that the along front wavenumber $l = l_0\exp(-\alpha T')$ and for the occluded front, $\overline{v}_s = \delta\overline{\zeta}_s = 0$ while $\overline{v}_n = (\overline{v}_{g5} - \overline{v}_{g3})\exp(-\alpha T')/2$. Another important parameter in these equations is the non-dimensional wavenumber 2μ. It is simply the product of the wavenumber and the width of the strip lL_e. In terms of the strip width in deforming geostrophic coordinates, L, $2\mu = l_0 e^{-2\alpha T'}(f/\overline{\zeta}_4)L = l^*L$. Furthermore, when $\delta\overline{\zeta}_n \cong \overline{\zeta}_4 - f$, it can be shown that $l_0\overline{v}_n/\delta\overline{\zeta}_n \cong \mu$.

Eq. (2.9) together with (2.5) define the development of frontal waves on the evolving vortex strip. Throughout this paper, solutions to (2.9)

were obtained using a fourth order Runge-Kutta integration scheme. Finally, readers may find the symbol table provided in Part 1, which concisely defines all the symbols introduced here, a useful reference in reading the rest of this paper.

3. Wave slope and its maximal amplification.

The work of DHJS suggests that wave disturbances on vortex strips are unlikely to induce non-linear processes such as vortex roll-up while the wave slope remains small. In this Section, we deduce the maximum possible amplification, $\mathcal{A}_m$, over a specified time, T_r of an approximation to the root mean square wave slope.

In Appendix A, we show that the order of magnitude of the displacement of the edges of the strip, ξ'_j, is related to $\tilde{Q}_j$ by the equation

$$O\left|\xi'_j\right| = O\left|e^{-\alpha T'}\mathcal{R}e\left[\tilde{Q}_j(T')\right]/\delta\bar{\zeta}_n\right|$$

where O indicates order of magnitude. Differentiating this equation with respect to y, one finds that

$$O\left|\frac{\partial\xi'_j}{\partial y}\right| = O\left|le^{-\alpha T'}\mathcal{R}e\left[\tilde{Q}_j(T')\right]/\delta\bar{\zeta}_n\right|. \qquad (3.1)$$

Noting from (2.7) that $\tilde{Q}_j$ is the integral of the perturbation vorticity across the transition region j multiplied by $\exp(\alpha T')$, one can see from (3.1) that the edge slope has the same order of magnitude as the integral of perturbation vorticity across the transition regions divided by the jump in basic state vorticity across these regions multiplied by the along front wavenumber. Thus, the implication of (3.1) is that in order for a wave to become non-linear the vorticity associated with the wave perturbation must (at least) amplify faster than the vorticity of the front itself. Since the increase of frontal vorticity approaches infinity as the front collapses to a discontinuity, the growth rate of a wave must match this extreme frontogenesis rate if it is to become non-linear. This indication of how

frontogenesis might damp non-linear mixing contrasts with the impression one might gain from Fig. 5 of Part 1 which illustrates how normal mode growth rates of the frontal are increased by frontogenesis. This apparent competition between stabilising and destabilising effects strongly motivated us to perform precise calculations to determine the conditions under which one or the other effects would dominate.

The mean square of the right hand side of (3.1) is

$$\Xi^2(T') = \frac{l}{2\pi} \int_0^{2\pi/l} \frac{l e^{-\alpha T'}}{\delta\bar{\zeta}_n} \frac{1}{2}\left\{\left[\mathcal{R}e\left(\tilde{Q}_3(T')\right)\right]^2 + \left[\mathcal{R}e\left(\tilde{Q}_5(T')\right)\right]^2\right\} dy \ ;$$

hence,

$$\Xi(T') = \frac{l_0 e^{-2\alpha T'}}{\delta\bar{\zeta}_n}\left[\frac{1}{2}\left(|\tilde{Q}_3|^2 + |\tilde{Q}_5|^2\right)\right]^{1/2}. \qquad (3.2)$$

Eq. (3.2) invites another interpretation of how frontogenesis reduces wave slope; *viz.*, the $\exp(-2\alpha T')$ term may be attributed to the wave flattening due to the cross front compression and along front lengthening due to the pure deformation $(-\alpha x, \alpha y)$ in the basic state wind while the $1/\delta\bar{\zeta}_n$ term is attributable to the cross-frontal compression caused by the convergence of the cross-frontal ageostrophic wind of the basic state.

We may now use (3.2) to express the amplification, $\mathcal{A}$, of wave slope over a specified time T_r as

$$\mathcal{A} = \exp(-2\alpha T_r)\ F\left(\frac{\delta\bar{\zeta}_n(0)}{\delta\bar{\zeta}_n(T_r)}\right) \qquad (3.3)$$

where

$$F = \left(\frac{|\tilde{Q}_3(T_r)|^2 + |\tilde{Q}_5(T_r)|^2}{|\tilde{Q}_3(0)|^2 + |\tilde{Q}_5(0)|^2}\right)^{\frac{1}{2}}.$$

Since F is the only parameter that depends on wave growth, for a given T_r, $\mathcal{A}$ is maximized whenever F is maximized. Since the governing eq. (2.6) is linear in Ψ' and any finite disturbance having zero vorticity outside

the transition regions, may be represented as a sum of two linearly independent solutions for Ψ'. It is easy to deduce the coefficients of two such functions in order to maximize F. As is evident from (2.5), a particular solution for Ψ' is characterized by its initial R value and as is evident from the RT diagrams presented in Part 1 (Fig. 6), any two solutions having different initial R values, denoted $R_1(T')$ and $R_2(T')$, will be linearly independent.

With $\delta\bar{\zeta}_s = 0$, (2.9b) predicts that if $R_1(0) = R_2^*(0)$ (where the * superscript denotes the complex conjugate) gives

$$R_1(T') = R_2^*(T') \tag{3.4a}$$

for all time. Using this result in (2.9a), one may also show that with $p_1(0) = p_2(0) = 0$,

$$\left(-il_0 p_1(T')\right) = \left(-il_0 p_2(T')\right)^*, \tag{3.4b}$$

for all time. We let these symmetry properties guide our choice of basis functions and let our first and second basis functions have initial R values $R_1(0) = -i$ and $R_2(0) = i$, respectively. An idea of the temporal behaviour of these modes may be gained from the RT phase diagrams presented in Part 1.

Denoting the $\tilde{Q}_j$ values associated with R_1, $\tilde{Q}_{31}$ and $\tilde{Q}_{51}$, and those associated with R_2, by $\tilde{Q}_{32}$ and $\tilde{Q}_{52}$, we may define *any* edge wave configuration in terms of a sum of these basis functions; *viz.*,

$$\tilde{Q}_3 = c_1\tilde{Q}_{31} + c_2\tilde{Q}_{32}, \tag{3.5a}$$

$$\tilde{Q}_5 = c_1\tilde{Q}_{51} + c_2\tilde{Q}_{52}, \tag{3.5b}$$

where

$$\tilde{Q}_{j1} = \left[(4 - j)iR_1 - 1\right]\exp\left\{il_0\left[Y' - p'_1(T')\right]\right\},$$

$$\tilde{Q}_{j2} = \left[(4 - j)iR_2 - 1\right]\exp\left\{il_0\left[Y' - p'_2(T')\right]\right\},$$

and where c_1 and c_2 are the coefficients of the basis functions associated

with R_1 and R_2, respectively.

Note that with $R_1(0) = -i$ and $R_2(0) = i$, the initial structures of the corresponding Ψ'_1 and Ψ'_2 waves have zero $\tilde{Q}_j$ at the west and east boundaries, respectively; i.e.

$$\tilde{Q}_{31}(0) = \tilde{Q}_{52}(0) = 0. \tag{3.6a}$$

Also note that the symmetries, (3.4), imply that at any T',

$$\tilde{Q}_{31} = \tilde{Q}_{52}^{*} \text{ and that } \tilde{Q}_{32} = \tilde{Q}_{51}^{*}. \tag{3.6b}$$

Using (3.5) in (3.3), gives F as a function of c_1 and c_2. For convenience, we normalise $\left(|\tilde{Q}_3(0)|^2+|\tilde{Q}_5(0)|^2\right)$ to unity by taking

$$c_1 = \frac{1}{2}\sin(\beta) \text{ and } c_2 = \frac{1}{2}e^{i\nu}\cos(\beta),$$

(the (1/2) is due to the fact that $|\tilde{Q}_{51}(0)| = |\tilde{Q}_{32}(0)| = 2$). The values of β and ν which maximize F for a given initial μ_0 and integration time T_r may then be determined by inspecting the derivatives of F with respect to β and ν; (cf. Bishop 1993b, for more details of the method).

The relationship between the maximal amplification of F, F_m, and the chosen basis functions is remarkably simple and is isomorphic to the expression for the optimal growth of strained baroclinic waves given in Bishop (1993b), *viz*,

$$F_m = \frac{1}{2}\left(|\tilde{Q}_{51}(T_r)| + |\tilde{Q}_{31}(T_r)|\right) \tag{3.7a}$$

or equivalently, (using (3.6b)),

$$F_m = \frac{1}{2}\left(|\tilde{Q}_{32}(T_r)| + |\tilde{Q}_{52}(T_r)|\right). \tag{3.7a}$$

Having normalised $\left(|\tilde{Q}_3(0)|^2+|\tilde{Q}_5(0)|^2\right)$ to unity, taking note of (3.6a) and comparing the forms of (3.3) and (3.7), it is evident that a theorem similar to the Triangle Inequality Theorem for vectors applies to edge wave amplification; *viz*,

The amplification of the sum of the squares of the edge wave amplitudes is less than or equal to the amplification of the square of the sum of

the edge wave amplitudes of a wave that initially had zero edge wave amplitude at one or the other boundaries.

The maximisation procedure reveals that the initial R value, $R_m(0)$, of the maximally amplifying wave is

$$R_m(0) = \frac{\sin(\lambda)}{1 + \cos(\lambda)}, \tag{3.8}$$

where

$$\lambda = \arg^*\left[\tilde{Q}_{51}(T_r)\tilde{Q}_{31}(T_r)\exp\left(-2il_0 p'_{r1}\right)\right]. \tag{3.9}$$

and p'_{r1} is the real part of p'_1. Note that since λ is real, $R_m(0)$ is real. From eq. (2.8), it may be deduced that if R is real then $\tilde{Q}_3$ and $\tilde{Q}_5$ have the same magnitudes. Furthermore, for waves on the occluded front, (2.9) can be used to show that if R is initially real it remains real for all time. Thus, (3.8) and (3.9) imply that the amplitudes of $\tilde{Q}_3$ and $\tilde{Q}_5$ are equal for maximally growing waves.

Furthermore, (2.8) can be used to show that the initial phase shift southward of the eastern vorticity wave relative to the western wave, $\Delta\chi_m(0)$, may be written

$$\Delta\chi_m(0) = 2\tan^{-1}\left(R_m(0)\right).$$

As we shall discuss later, the $\Delta\chi$ value of optimally growing short wavelength initially decreases and sometimes passes through -180^0 before the end of the time, T_r. When this happens, it is meaningful to say that the western wave has overtaken the eastern wave. To include this information in our expression for the optimal initial phase shift, we let n equal the number of times the $\Delta\chi$ value of an optimally growing wave is observed to pass through -180^0 over the time T_r and then set

$$\Delta\chi_m(0) = 2\tan^{-1}\left(R_m(0)\right) + n\times 180. \tag{3.8}$$

In the following section, we use the aforementioned equations to

investigate the nature of maximally growing waves and hence the stability of an evolving front.

4. The parameter space of maximal amplification.

A fundamental assumption of stability theory is the existence of an "initial disturbance". Conceivably, such disturbances could enter the frontal vortex strip at any time during the development of the front. In recognition of this we take $\mathcal{A}_m$ to be a function not only of the strain rate, α, *but also* of the time of entry, T_e, the non-dimensional wavenumber $2\mu_0(T_e)$ at the time of entry and the residence time, T_r, of the waves on the front. Note that $T_e = 0$ denotes an entry time when the relative vorticity in region 4 is equal to the planetary vorticity.

In order to gauge the amount by which a wide range of disturbances can grow on the front, we shall define and calculate a number of different extrema of the function $\mathcal{A}_m$. Firstly, we set $T_e = 0$ and use $\mathcal{A}_1[\alpha, 0, 2\mu_0(0)]$ to denote the surface of maximum values of $\mathcal{A}_m[\alpha, T_e, 2\mu_0(T_e), T_r]$ over the range of residence times T_r between 0 and t_{wk}, where t_{wk} is the time at which the assumption of laminar, inviscid flow is deemed to be untenable due to the extremely strong frontal gradients.

Unfortunately, available theoretical bases for deducing what this t_{wk} might be are still in their infancy. Also, Appendix A of Part 1 suggests that thermal wind balance will breakdown when both the vorticity and the strain rate are high. At such times, the model's rate of frontal intensification is likely to be unrealistic. Nevertheless, since we wish to illustrate how much an idealisation of frontogenesis can stabilize wave growth and since normal mode theories give growth rates proportional to vorticity, we overestimate the vorticity value at which our model becomes

inaccurate and take t_{wk} to be the time at which $\partial \bar{v}_g / \partial x$ reaches $64f$. Assuming that the initial relative vorticity is equal to f at $T_e = 0$, $t_{wk} = 9.41$ hrs/($\alpha \times 10^5 s$). The T_r and $\Delta\chi_0$ values which produce the $\mathcal{A}_1$ surface will be denoted T_{r1} and $\Delta\chi_{01}$, respectively.

Having found how, with T_e=0, strain affects disturbance growth at different wavenumbers, we shall investigate how changes in the entry time of disturbances affect growth by calculating the maximum values of $\mathcal{A}_m$ with respect to both T_r and $2\mu_0(T_e)$, for a range of T_e and α[1]. This maximum will be denoted by $\mathcal{A}_2(\alpha, T_e)$ and the values of T_r, $\Delta\chi(T_e)$ and $2\mu_0(T_e)$ associated with it will be denoted T_{r2}, $\Delta\chi_{02}$ and $2\mu_{02}$, respectively. Finally, we shall focus our attention on the maximum of $\mathcal{A}_2$ over T_e, $\mathcal{A}_3(\alpha)$ and denote the parameters defining it by T_{r3}, $\Delta\chi_{03}$, $2\mu_{03}$ and T_{e3}.

In summary:

* $\mathcal{A}_m[\alpha, T_e, 2\mu_0(T_e), T_r]$ is the maximum possible amplification, in the time T_r, of a wave which on entering the frontal zone at T_e has the non-dimensional wavenumber $2\mu_0(T_e)$ and is subject to strain of strength α.

* $\mathcal{A}_1[\alpha, 0, 2\mu_0(0)]$ is the maximum of $\mathcal{A}_m$ with respect to the residence time for $T_e = 0$. (cf. Fig. 3)

* $\mathcal{A}_2(\alpha, T_e)$ is the maximum of $\mathcal{A}_m$ with respect to the residence time and the non-dimensional wavenumber at the time of entry. (cf. Fig. 5)

* $\mathcal{A}_3(\alpha)$ is the maximum of $\mathcal{A}_2$ with respect to the time of entry; (cf Fig. 6).

[1]While the expressions of § 3 apply directly to the $T_e = 0$ entry time, the argument is equivalent for any entry time and the appropriate maximal amplification equations for $T_e \neq 0$ are obtained from those in § 3 by simply replacing T=0 by T=T_e.

5. Description and interpretation of the effect of strain on growth.

Fig. 1a, in depicting $\mathcal{A}_1(\alpha,\ 0,\ 2\mu_0(0))$, shows how strain affects the maximal growth of $T_* = 0$ disturbances. The $\mathcal{A}_1(1.0\times10^{-5}s^{-1},\ 0,\ 2\mu_0(0))$ curve lies coincident with the $\ln(\mathcal{A}) = 0$ line as, remarkably, this strain rate is enough to *completely* suppress wave steepening. The other curves show how weaker strain rates allow more growth. For $\alpha = 0.8\times10^{-5}s^{-1}$ and $0.6\times10^{-5}s^{-1}$ maximum growth occurs at infinite wavelength. The $\alpha = 0.4\times10^{-5}s^{-1}$ curve has two peaks one at infinite wavelength the other at $2\mu_0(0) = 1.92 \pm 0.025$. The types of growth occurring at these two peaks may be distinguished by diagnosing the type of edge wave interaction[2] causing the growth.

A simple way of doing this is to (a) write $\tilde{Q}_3$ and $\tilde{Q}_5$ in the form

$$\tilde{Q}_3 = -2Cl_0\cos\left[l_0Y' + \mathcal{P}_3(T')\right]\exp[\gamma_3(T')], \tag{5.1}$$

$$\tilde{Q}_5 = -2Cl_0\cos\left[l_0Y' + \mathcal{P}_3(T') + \Delta\chi\right]\exp[\gamma_5(T')], \tag{5.2}$$

where γ_5, γ_3, $\mathcal{P}_3$ and $\Delta\chi$ are strictly real; (b), use (2.7) to deduce the streamfunction field induced by each of these waves, (c) deduce the time rate of change γ_5, γ_3, $\mathcal{P}_3$ and $\Delta\chi$ by substituting the expressions for the $\tilde{Q}_j$ waves and their induced streamfunction fields into (2.6). Details are provided in Appendix B. As mentioned in § 3, for the occluded front, the fastest growing waves have equal amplitudes in regions 3 and 5, i.e, $\gamma_5 = \gamma_3 = \gamma$; for such waves (B.4) shows that γ is controlled by

$$\frac{\partial\gamma}{\partial T'} = (\delta\bar{\zeta}_n/2)\ \exp(-2\mu)\ \sin(\Delta\chi). \tag{5.3}$$

Thus, in accord with the ideas of Bretherton (1966), growth is proportional to the product of a scale term S, equal to $\exp(-2\mu)$, and a phase term, P, equal to the sine of the counter shear phase difference between the two vorticity waves. Whilst actual optimal growth represents the maximal value

[2]A more detailed discussion of edge or Rossby wave diagnostics is presented in Bishop (1993b).

of the time integral of the product of S and P, some insight can be gained by considering what sort of structures would maximize the time integral of just S or P alone. Obviously, ultra long waves maximize S and the μ_0=0 peak on the $\alpha = 0.4\times10^{-6}s^{-1}$ curve must partially be a result of this fact. The structures likely to optimize the time integral of P are those that allow $\Delta\chi$ to remain near 90^0. Subtracting (B.4b) from (B.4d) one finds that the eq. for $\Delta\chi$ corresponding to (5.3) is

$$\frac{\partial(\Delta\chi)}{\partial T'} = \delta\bar{\zeta}_n\left[1 - 2\left(\frac{l_0\bar{v}_s}{\delta\bar{\zeta}_n}\right) + \exp(-2\mu)\cos(\Delta\chi)\right]. \qquad (5.4)$$

An analysis of this eq. shows that there is a μ_L and μ_U such that for $\mu > \mu_U$, $\partial(\Delta\chi)/\partial T' < 0$ for any $\Delta\chi$ and that for $0 < \mu < \mu_L$, $\partial(\Delta\chi)/\partial T' > 0$; i.e. if $d\mu/dT'$ was zero then for $\mu > \mu_U$ the two vorticity waves would be continually advected past each other in a cyclonic sense, whereas if $0 < \mu < \mu_L$ they would propagate past each other in an anticyclonic sense[3]. If $\mu_L < \mu < \mu_U$ and if $\Delta\chi_{nm}$ is the positive value of $\Delta\chi$ that makes $\partial(\Delta\chi)/\partial T' = 0$, then provided that $\Delta\chi \neq -\Delta\chi_{nm}$, $\Delta\chi$ is always attracted toward $\Delta\chi_{nm}$. This attraction is graphically illustrated in Fig. 8 of Part 1 for the special case of waves with $2\mu_0(0) = 2.1$ and $\Delta\chi_0 = 179^0$. Also, μ_L and μ_U respectively correspond to the long and short wavelength cut offs for the normal mode instabilities that would be supported by the front if the deformation was switched off. The normal mode characteristics of a cold front whose stability characteristics are very similar to the warm front studied here are illustrated in Fig. 5(a) of Part 1.

Setting $\partial(\Delta\chi)/\partial T' = 0$ in (5.4) and solving for $\Delta\chi_{nm}$ yields

$$\Delta\chi_{nm} = \left|\cos^{-1}\left\{\left[2\left(\frac{l_0\bar{v}_s}{\delta\zeta}\right) - 1\right]\exp(2\mu)\right\}\right|$$

[3]Note that when $\delta\bar{\zeta}_n$ tends to $\partial\bar{v}_s/\partial x$, $l_0\bar{v}_n/\delta\bar{\zeta}_n$ tends to μ and, consequently, μ_L tends to zero.

$$\equiv \left|\cos^{-1}\left\{\left[2\mu - 1\right]\exp(2\mu)\right\}\right|. \qquad (5.5)$$

Thus, $\Delta\chi_{nm}$ will be near 90^0 whenever 2μ is near 1. Such wavelengths allow $\Delta\chi$ to remain near 90^0 longer than any other. Since 2μ monotonically decreases with time, growth peaks at $2\mu_0$ values larger than 1 partially result from increasing the time integral of the phase term. Note that such increases in the time integral of *P* are obtained at the expense of *S* which decreases exponentially with 2μ. For future reference, when growth results mainly from a maximization of the *S* or *P* term, we shall refer to such growth as "*S* type" or "*P* type" growth, respectively. Thus, the $2\mu_0$=0 and the $2\mu_0$ = 1.92 peaks on the $\alpha = 0.4\times10^{-5}s^{-1}$ curve are characterized by *S* type and *P* type growth, respectively.

As we shall see, the variation of *P* type growth with both wavenumber and entry time may be understood in terms of a trade-off between enhancing growth by keeping $\Delta\chi$ near 90^0 for as long as possible and the possible growth enhancement achievable by letting $\Delta\chi$ be near 90^0 when the vorticity of the strip is very high. The *RT* diagrams of Part 1, together with (5.4) and (5.5) tell us that when the 2μ value of a wave is equal to 1, the mutual interaction of the edge waves favours a counter shear phase shift of 90°. Thus, if the 2μ value of a wave reduces to 1 at a time when the vorticity of the wave is very high, its *P* type growth will be proportionally higher. However, as the dashed lines on Fig. 2 show, 2μ decreases as the vorticity (or $T_n = T'/t_c$) increases; consequently, waves whose 2μ value becomes equal to one when the vorticity is high begin their development at a very high wavenumber where sustained growth is impossible. Also, as the vorticity (or T_n) becomes larger the period of time over which 2μ equals one becomes shorter and furthermore, if 2μ reduces to unity just

before frontal collapse there will simply not be enough time available for significant *P*-type growth to be realised. Nevertheless, there will always be a strain rate small enough to ensure that there is enough time for the extremely large growth rates achievable by late developing waves to produce net wave steepenings in excess of those which develop earlier. The implication of this is seen in Fig. 1a; *viz*, as the strain rate is reduced, the net growth of short wavelength waves increases.

It is possible to use our edge wave diagnostics to give these ideas a quantitative basis. It is of more than passing interest to do so, since, as we shall see, the relevant mathematical expressions give rise to a strict upper bound on the growth rates of frontal waves.

Differentiating the natural log of (3.3) and using (5.3) leads to

$$\frac{\partial[\ln(\mathcal{A})]}{\partial T'} = \frac{\partial \gamma}{\partial T'} - 2\alpha - \frac{d[\ln(\delta\bar{\zeta}_n)]}{dT'}$$

$$= (\delta\bar{\zeta}_n/2)\, e^{-2\mu}\sin(\Delta\chi) - \frac{2\alpha}{f}\left(\bar{\zeta}_2 + \bar{\zeta}_4\right). \qquad (5.6)$$

The last term in this equation is negative definite and is proportional to (α/f). Since $\left(\bar{\zeta}_2 + \bar{\zeta}_4\right)$ always has the same order of magnitude as $\delta\bar{\zeta}_n/2$ we have the rather general result that:

There is always a strain rate that can completely suppress wave steepening. This is true even when the front has a structure which, in the absence of strain, would support infinite normal mode growth rates.

Thus, (5.6) shows that, in principle, there is always a strain rate capable of suppressing barotropic mixing and hence of allowing the front to collapse to a discontinuity provided other mixing processes do not become active.

By maximising the first term on the right hand side of (5.6) by setting $2\mu = 0$ and $\Delta\chi = 90^0$, using (2.3) and (2.4) and noting that infinite

vorticity is reached when $\exp(2\alpha T') = 1/E_4$, one can show that the minimum strain rate, α_{min}, required to entirely prohibit growth is given by

$$\alpha_{min}(\alpha T', 2\mu) = \frac{f}{4}\left(\frac{\bar{\xi}_4 - \bar{\xi}_2}{\bar{\xi}_4 + \bar{\xi}_2}\right) e^{-2\mu}. \qquad (5.7)$$

Thus, as the front intensifies larger strain rates are needed to suppress wave steepening. At the point of frontal collapse (when the vorticity is infinite !) all frontal wave steepening is suppressed if $\alpha/f \geq 1/4$.

The variation of α_{min} on the $(T_n, 2\mu)$ plane is illustrated in Fig. 2. The evolution of a variety of different non-dimensional wavenumbers with T_n is also depicted on this diagram. Note the increase and decrease of α_{min} with T_n and 2μ, respectively. The diagram shows how, as was mentioned previously, a wave with an initially large wavenumber is bound to decay until the strain rate required to completely suppress growth becomes larger than the strain rate acting on the front.

For example consider a frontal wave which at $T_n = 0$ had $2\mu = 3.0$ and is developing in a strain rate of $0.2\times10^{-5}s^{-1}$. Tracing down the corresponding dashed 2μ isoline reveals that it is not until T_n becomes greater than about 0.32 that the 2μ curve for this wave crosses the $\alpha_{min} = 0.2\times10^{-5}s^{-1}$ isoline. Thus, growth only becomes possible once T_n becomes greater than about 0.32. At this time the 2μ value of the wave equals 1.8 and hence, the wave is poised to experience *P* type growth on a relatively intense front and there is $t_c(t_{wk}/t_c - 0.32) = 31.6$ hr left before the integration is stopped. Fig. 3a indicates that waves with approximately this wavelength can grow faster than all others. Thus, the example illustrates how early decay can be compensated for by waves whose wavelengths allow them to experience *P* type growth at a time when the front is relatively intense.

Fig's 1b - 1d show the residence times, T_{rl}, and initial phase shifts,

$\Delta\chi_{01}$, corresponding to the A_i curves as a function of $2\mu_0$. As would be expected from the fact that at large wavelengths $\partial(\Delta\chi)/\partial T' > 0$, maximal *S* type growth occurs with $\Delta\chi_{01}$ less than 90^0 and with T_{r1} about half of t_{wk}. Such initial phase shifts allow the waves to achieve a 90^0 phase shift at some stage of their development. Conversely, since at $2\mu > 1$ we have $\partial(\Delta\chi)/\partial T' < 0$ for $\Delta\chi > 90^0$, maximal *P* type growth usually occurs with $\Delta\chi_{01}$ greater than 90^0 and with T_{r1} considerably more than half of t_{wk}. Note that whilst the *P* type waves begin development with $\partial(\Delta\chi)/\partial T' < 0$, the basic state flow forces their non-dimensional wavenumber to rapidly decrease; consequently, they end their development like *S* type waves with $\partial(\Delta\chi)/\partial T' > 0$.

Fig's 1c and 1d indicate that as α increases $\Delta\chi_{01}$ becomes closer to 90^0 for both *S* and *P* type waves. This might have been expected on the grounds that the range of $\Delta\chi$ over a fixed non-dimensional time period, $\alpha T'$, gets smaller as α increases. Consequently, with a smaller $\Delta\chi$ range at large α, $\Delta\chi$ must start nearer 90^0 in order to stay near 90^0 during development.

A striking feature of Fig. 1c is the very large initial counter shear phase shifts at short wavelengths. For example, for $\alpha = 0.2\times10^{-5}s^{-1}$, the initial counter-shear phase shift of the fastest growing wave is at $(720+184)^0$; (occurs at $2\mu_0(0) = 3.32$). Thus, the vorticity wave on the east boundary moves more than two wavelengths north of the vorticity wave on the west boundary before locking on. During this overtaking phase the non-linearity of the wave actually decreases with time. This can be seen from Fig. 2 which shows that growth cannot occur until $2\mu \cong 1.8$ and $T' \cong 0.35\ T_n$. As mentioned previously, this initial decrease in waveslope is compensated for by the rapid *P* type growth that can occur at the time when 2μ is near 1 and the front is intense.

Initial decay periods can be avoided by letting the front be disturbed at a later time in its evolution. This helps explain why, as is illustrated by the $\alpha = 0.2\times10^{-5}s^{-1}$ and $0.4\times10^{-5}s^{-1}$ curves for $\mathcal{A}_2(\alpha, T_e)$ on Fig. 3a, *P* type growth increases with T_e until T_e becomes so close to t_{wk} that there is simply not enough time left for significant growth to occur.

Fig's 3b and 3c detail the variation with T_e of the initial horizontal structure parameters, $2\mu_{02}$ and $\Delta\chi_{02}$, respectively. Note that for $\alpha = 0.2\times10^{-5}s^{-1}$, it only takes a small increase in T_e for the *P* type growth of the large $2\mu_{02}$, "overtaking" type modes to be surpassed by the *P* type growth of the smaller $2\mu_{02}$ "non-overtaking" modes. This characteristic is because (a), even with $T_e = 0$, the growth of the large $2\mu_{02}$ modes only slightly exceeds the non-overtaking growth peak near $2\mu_{02} = 1.9$ and (b), as T_e increases, the $2\mu_{02}$ near 1.9 become subject to higher $\delta\bar{\zeta}_n$ values at the time when $\Delta\chi_n = 90^0$.

The $\alpha = 0.8\times10^{-5}s^{-1}$ and $1.0\times10^{-5}s^{-1}$ curves in Fig's 3(a) and (c) indicate that *S* type growth also increases with T_e. For $\alpha = 0.6\times10^{-5}s^{-1}$, *P* type growth exceeds *S* type growth for T_e between 11.0 and 14.5 hrs, only. This indicates that the increase of *P* type growth with T_e is greater than that of *S* type growth.

The maximum possible *P* type growth over all possible T_e for strain rates between $0.2\times10^{-5}s^{-1} < \alpha < 0.6\times10^{-5}s^{-1}$ is described in Fig. 4a. Since at $\alpha=0.6\times10^{-5}s^{-1}$ maximal *P* type growth is only slightly less than maximal *S* type growth, this curve is approximately equivalent to $\ln[\mathcal{A}_3(\alpha)]$. The initial and final dimensional wavelengths of these waves are depicted in Fig. 4b. These dimensional wavelengths, λ_d, were calculated using

$$\lambda_d = \frac{\pi}{\mu} L_c = \frac{\pi}{\mu} Le^{-\alpha T'} (f/\bar{\zeta}_4)$$

An examination of the governing eq's shows that our stability analysis is

almost independent of L, provided the evolution of the vorticity is unchanged[4]. Thus, in considering Fig. 4b, one should bear in mind the dependence of the dimensional wavelengths shown on our geophysically relevant but otherwise arbitrary choice of L. A general result evident from Fig. 4b and not dependent on our choice of L is the fact that the dimensional wavelengths of the fastest growing waves are relatively unaffected by the strain rate.

6. Scale Selection

The extent to which a shear flow can "select" certain wavelengths out of a broad spectrum of background noise depends on its ability to grow one particular wavelength more than another before any of these other waves become non-linear. Fig. 1a shows that with $\alpha = 0.2\times10^{-5}s^{-1}$, our shear flow can produce amplifications > 70 for wavelengths shorter than $(2\pi/1.7)\times L_{c0}$ and longer than $(2\pi/6.0)\times L_{c0}$ where L_{c0} is the Cartesian width of the vortex strip at the time (T_e=0) when the vorticity was equal to f. For the occluded front considered here, L_{c0} = 173 km. Thus, if for all μ and entry times, the waveslope, Ξ, was such that $0.02 < \Xi(T_e) < 0.1$, all wavelengths shorter than 640 km and longer than 181 km could produce $\Xi(T_r) > 0.1$. However, since longer wavelengths have their rapid growth period earlier than shorter wavelengths, it is possible that they could prevent potentially faster growing short wavelengths from developing by inducing vortex roll-up before the shorter wavelengths entered their rapid growth phase. If this did not occur then a situation (similar to that described by Grabowski and Clark 1991) might develop whereby an initially monochromatic disturbance is disturbed late in the life of the front as a shorter

[4]With reference to Part I, the temporal dependence of the low-level vorticity of region 4 is unchanged by L provided that Λ/L is kept constant.

wavelength mode grows over it.

With $\alpha = 0.4\times10^{-5}s^{-1}$, $\mathcal{A}_3 = 2.3$ so that with $0.05 < \Xi(T_e) < 0.1$, only a relatively short band of wavelengths near 200 km will be capable of making $\Xi(T_f) > 0.1$. With $\alpha = 0.6\times10^{-6}s^{-1}$ the width of the band of wavelengths around 175 km capable of making $\Xi(T_f) > 0.1$ will be even narrower. For $\alpha > 0.6\times10^{-5}s^{-1}$ the very small optimal growth rates indicate that frontal waves are incapable of significantly changing their slope.

7. Discussion.

The stability analysis of a simplified moist front suggests that the steepening of waves on frontal potential vorticity strips is strongly suppressed by frontogenesis. The ($u=-\alpha x$, $v=\alpha y$) part of the flow tends to flatten frontal waves by compressing them and extending them in the cross and along front directions, respectively. The cross-front amplitude is also compressed by the ageostrophic circulation. This circulation increases the vorticity at the front whilst decreasing the width of the vorticity strip. The enhancement of frontal wave growth that would result from the vorticity increase is offset by the effect of the narrowing of the vortex strip on the coupling between the vorticity waves on either side of the strip. Thus, the net effect of these processes inhibits the genesis of non-linear frontal waves. The present work quantifies these effects for an idealized front.

A semi-analytic expression for the optimal growth of the root mean square of frontal wave slope during frontogenesis has been obtained. With this expression, the ability of frontogenesis to suppress wave steepening has been explored. The results have been interpreted with the aid of diagnostics which quantify Bretherton's (1966) counterpropagating edge (or Rossby) wave view of shear instabilities. They show that growth is

proportional to a scale term which increases with the wavelength and a phase term which is equal to the sine of the countershear phase shift of the two edge waves. This leads us to distinguish between *S* type optimal growth which is achieved by maximising the scale term at the expense of the phase term and *P* type optimal growth which is achieved by keeping the two edge waves in a growth configuration as long as possible at the expense of the scale term. The *P* type growth is more strongly affected by frontogenesis than *S* type growth because it depends on an approximate counter balance between the propagation speeds of edge waves and the advective effects of the cross-frontal shear. It is this counterbalance which is strongly affected by the rapid change in the ratio of wavelength to frontal width produced by frontogenesis.

The edge wave diagnostics also lead to an expression for the minimum strain rate required to completely prevent wave steepening at any given time or wavenumber. This minimum strain rate increases with wavelength and with the vorticity of the frontal vortex. Remarkably, at the point of frontal collapse, when the vorticity of the front is infinite and the associated normal modes have infinite growth rates, it only takes a strain rate of $f/4$ to annihilate the possibility of wave steepening at *any* wavelength. (It is intriguing to note the similarity of DHJS's corresponding result that steepening on a purely barotropic vortex strip is completely suppressed for $\alpha/(\bar{\xi}_4 - f) = 1/4$ (our notation)).

The diagnostics help explain why it is necessary that waves experiencing *P* type optimal growth must experience initial decay in order to have non-dimensional wavelengths well suited for growth at a later time when the vorticity of the front is very high. Letting the disturbance enter the front at a later time removes these initial decay periods and this

accounts for the simulated increase in wave steepening as the time at which the disturbance is assumed to enter the front is increased.

One can speculate that although frontogenesis acts to suppress frontal waves it also acts to allow the potential instability to develop. This is analogous to deep convection where an inversion will cap the boundary layer for a period during which the moisture content and potential instability increase markedly. When the inversion dissipates, deep convection is triggered. Similarly, during moist frontogenesis frontal waves are suppressed while the moist circulation intensifies the potential vorticity and hence the potential instability of the strip. If later in the frontal lifetime the frontogenesis is diminished, frontal wave instability is triggered.

It is mainly the presence of ageostrophic convergence which distinguishes the vortex strip studied in this paper from that examined in DHJS. It is tempting to attempt to isolate the damping effect of ageostrophic convergence on instability by comparing the present results with those of DHJS. This cannot be done because, whilst the vorticity of their strip is constant, in our case the vorticity rapidly amplifies. Thus, since amplification rates are proportional to the vorticity, the "potential" wave amplification of two strips with or without ageostrophic convergence is different. A better way of isolating such affects is discussed in Bishop (1993b).

It is of interest, however, to note that in the absence of ageostrophic convergence, the slope of waves on a frontal vortex strip with vorticity equal to $4f$, subject to a strain rate $\alpha = 1\times10^{-5}s^{-1}$ could amplify 244 times in 44 hrs (cf. Fig. 4 of DHJS). Our experiments show that when an equivalent strain rate acts on our idealized thermal structure, frontal

waves can only steepen by a factor of 1.8. Note however that barotropic type instability is not the only source of frontal waves and that the results in Bishop (1993b) suggest that baroclinic growth would not be damped by strain nearly as much as the barotropic growth discussed here.

The role of non-zero low-level wind shears may be included in our model by letting the lowest kilometer behave like an Ekman type boundary layer; the kilometer above this layer then remains as the barotropic seat of frontal wave development. Calculations (not presented here) show that the main difference this boundary layer introduces is that the height Z_c at which $\partial\bar{\psi}/\partial Z$ is zero is lowered. Thus, if for the same reasons as for the inviscid basic state, we take $v_g(X',Z_c,0) = 0$, the evolution of vorticity above the boundary layer has the same dependence on $\alpha T'$ as that for the inviscid basic state. Consequently, the stability characteristics are found to be equivalent to those of the inviscid basic state. Note however that such simplified boundary layers appear to significantly affect the stability of the strip when the strain rate is allowed to vary in time; this will be discussed in future work.

In certain circumstances measures of frontal wave growth other than the amplification of non-linearity will be more useful. For example, one might be more interested in the growth of the perturbation horizontal streamfunction. Fig. 5 shows the maximum possible amplification of streamfunction amplitude for waves entering the frontal zone at $T_0 = 0$, over a variety of non-dimensional wavenumbers. Notable differences to the corresponding amplification of wave slope, (cf. Fig. 1a), include: (a) the complete absence of long wavelength *S* type growth and a shifting of *P* type growth peaks to even shorter wavelengths and (b) whilst possible growth still decreases as the strain rate is increased, significant *P* type growth

now occurs for all strain rates.

The significant long wave *S*-type growth of edge waves is not apparent in the streamfunction field because of superposition effects. For *S*-type growth the eastern and western edge waves are initially in phase with each other. In this configuration, the streamfunction field induced by the eastern wave reinforces that induced by the western wave. As the edge waves grow, however, they become more and more out of phase with each other. Their growth ceases when they become 180^0 out of phase with each other. In this configuration the induced streamfunction fields cancel each other out. Apparently, the transition of the edge waves from a configuration where their induced streamfunction fields are superposed to one where the induced fields cancel each other out cancels the net growth in the streamfunction field that might have been associated with the edge wave growth alone.

The present work is also relevant to that of Grabowski and Clark (1991) who made numerical investigations of wave growth on the intensifying shear layer of a buoyant bubble. In particular, it provides a precise description of the process they refer to (cf. their p.543) whereby smaller scale disturbances are selected at a later time during the intensification of a shear zone.

Our prediction that low-level frontal waves should occur on a wide variety of horizontal scales is confirmed by the climatology of extratropical cyclone sizes compiled by Nielson and Dole (1991). They also find that the size of cyclones has some relationship to their age and that typically, in the initial stages of development, "two small scale cyclones are located along a front, separated from each other by 450 km..". Since stability studies indicate that baroclinic type frontal waves have a preferred scale somewhat larger than this (~ 1000 km, cf Joly and Thorpe

(1991)), it seems likely that the 450 km waves observed by Nielson and Dole (1991) may have amplified via a barotropic mechanism similar to that examined here. The same could be said of the 100 km wave observed by Neiman et. al. (1991).

To conclude, the prototype model predicts that transitions from linear to non-linear development are most likely to occur when the strain rate is small and that the wavelength at which non-linear development occurs is likely to decrease as the strain rate increases. Transitions from linear to non-linear development are very unlikely when the strain rate exceeds $0.6\times10^{-5}s^{-1}$. The results support the hypothesis that atmospheric frontogenesis rates are capable of strongly reducing the mixing efficiency of barotropic eddies. In doing so, they describe how moist frontogenesis can create flows which would, if the frontogenesis ceased, be strongly unstable. To test these propositions against observations, a counterpart to the model's horizontal deformation field must be identified in the data. This problem will be addressed in a subsequent publication.

Acknowledgements.

In preparing this paper, the authors benefited from discussions with Martin Juckes. One of the authors (Craig Bishop) was financially supported by a Natural Environment Research Council Grant (GR3/6920).

APPENDIX A: Relationship between strip displacement and $\tilde{Q}_j$.

In this Appendix, we obtain the relationship between $\tilde{Q}_j$ and the position of the edges of the strip ξ_j by

(a) finding the relationship between u'_r and the Lagrangian derivative of ξ_j;

(b) using this result in (2.6) which relates the Lagrangian evolution of $\tilde{Q}_j$ to the perturbation velocity u'_r and

(c) integrating (2.6) with respect to time following the along front flow.

The relationship between u'_r and the x-component of the velocity of the edges can be found by noting that since $\partial x/\partial X' = \exp(-\alpha T')f/\bar{\zeta}_4$, the x-coordinate of the edges in Cartesian space, ξ_j, can be expressed without loss of generality as

$$\xi_j = e^{-\alpha T'}\left(f/\bar{\zeta}_4\right)\left(\frac{L}{2}(j-4)+\eta_j\right), \tag{A.1}$$

where η_j is the displacement of the edges in deforming geostrophic coordinates from their undisturbed position and j equals either 3 or 5 depending on the transition region referred to. We can then relate η_j to u'_r by noting that the total zonal wind at the edges of the vortex strip is equal to the Lagrangian derivative of ξ_j. Comparing the expression for this speed given by (2.1) gives with the one derivable from (A.1) yields

$$-\alpha\xi_j + \bar{u}_a + u'_r = \frac{D\xi_j}{Dt} = -\alpha\xi_j + e^{-\alpha T'}\left((j-4)\frac{L}{2}+\eta_j\right)\frac{D(f/\bar{\zeta}_4)}{DT'} + e^{-\alpha T'}\left(f/\bar{\zeta}_4\right)\frac{D\eta_j}{DT'}. \tag{A.2}$$

Using (2.2) and the fact that $f/\bar{\zeta}_4 = \left[1 - \exp(2\alpha T')\ E_4\right]$ where $\exp(\alpha T')\ E_4 = (1/f)\partial\bar{v}_g/\partial X'$, it is evident that

$$e^{-\alpha T'}\left((j-4)\frac{L}{2}+\eta_j\right)\frac{D(f/\bar{\zeta}_4)}{DT'} = -2\alpha\bar{v}_g(\xi_j,t)/f = \bar{u}_a(\xi_j,t).$$

Thus, this expression together with (A.2) implies that

$$u'_r = e^{-\alpha T'}\left(f/\bar{\zeta}_4\right)\frac{D\eta_j}{DT'} \cong e^{-\alpha T'}\left(f/\bar{\zeta}_4\right)\frac{\bar{D}\eta_j}{\bar{D}T'} \qquad (A.3)$$

where the approximate equality in (A.3) comes from the neglect of non-linear terms in the Lagrangian derivative. This leads to a linear prediction of the position of the edges.

The simple relationship between η_j and $\tilde{Q}_j$ may now be seen by using (A.3) in (2.6) to obtain

$$\frac{\bar{D}\eta_j}{\bar{D}T'} = -(4 - j)\left(\frac{\bar{\zeta}_4}{f\delta\bar{\zeta}_n}\right)\frac{\bar{D}\tilde{Q}_j}{\bar{D}T'} . \qquad (A.4)$$

Integrating this equation with respect to time following the basic state flow from T'_0 to T' and setting

$$\eta_j(T'_0)/(4 - j) = - \left[\tilde{Q}_j\left(\bar{\zeta}_4/(f\delta\bar{\zeta}_n)\right)\right](T'_0)$$

yields

$$\eta_j(T')/(4 - j) = - \left[\tilde{Q}_j\left(\bar{\zeta}_4/(f\delta\bar{\zeta}_n)\right)\right](T') + \int_{T'_0}^{T'} \tilde{Q}_j \frac{\bar{D}\left(\bar{\zeta}_4/(f\delta\bar{\zeta}_n)\right)}{DT'} DT' . \qquad (A.5)$$

Note that since the $\tilde{Q}_j$ value of a growing wave will reach its maximum amplitude at the final time T', it follows that

$$\int_{T'_0}^{T'} \tilde{Q}_j \frac{\bar{D}\left(\bar{\zeta}_4/(f\delta\bar{\zeta}_n)\right)}{DT'} DT' \le \left|\tilde{Q}_j(T')\right| \int_{T'_0}^{T'} \frac{\bar{D}\left(\bar{\zeta}_4/(f\delta\bar{\zeta}_n)\right)}{DT'} DT' < \left|\tilde{Q}_j(T')\right|/f. \qquad (A.6)$$

Since the last term in (A.6) is smaller than the amplitude of the first term in (A.5), $(\bar{\zeta}_4/\delta\bar{\zeta}_n > 1)$, it follows that

$$O\left|\eta_j(T')\right| = O\left|\left[\tilde{Q}_j\left(\bar{\zeta}_4/(f\delta\bar{\zeta}_n)\right)\right](T')\right| . \qquad (A.7)$$

Thus, denoting the displacement of the edges from their equilibrium positions by ξ'_j, (i.e. $\xi'_j = \mathcal{R}e\left[\xi_j(T') - (j - 4)L_c/2)\right]$, (A.7) may be used in (A.1) to show that

$$O\left|\xi'_j\right| = O\left|e^{-\alpha T'}\tilde{Q}_j/\delta\bar{\zeta}_n\right| . \qquad (A.8)$$

APPENDIX B: Edge wave dynamics.

The cartesian forms

$$\Psi'_3 = \begin{cases} -(\tilde{Q}_3/2l_0)\exp\left[-l\left(\frac{L_c}{2} + x\right)\right] & \text{for } x \geq -\frac{L_c}{2}, \\ -(\tilde{Q}_3/2l_0)\left\{1 + \frac{l\delta L_c}{\pi}\cos\left[\frac{\pi}{\delta L_c}\left(\frac{L_c}{2} + \frac{\delta L_c}{2} + x\right)\right]\right\} & \text{for } -\frac{L_c}{2} \geq x \geq -\frac{L_c}{2} - \delta L_c, \\ -(\tilde{Q}_3/2l_0)\exp\left[l\left(\frac{L_c}{2} + \delta L_c + x\right)\right] & \text{for } x \leq -\frac{L_c}{2} - \delta L_c, \end{cases} \quad \text{(B.1a)}$$

and

$$\Psi'_5 = \begin{cases} -(\tilde{Q}_5/2l_0)\exp\left[-l\left(\frac{L_c}{2} - x\right)\right] & \text{for } x \leq \frac{L_c}{2} \\ -(\tilde{Q}_5/2l_0)\left\{1 + \frac{l\delta L_c}{\pi}\cos\left[\frac{\pi}{\delta L_c}\left(\frac{L_c}{2} + \frac{\delta L_c}{2} - x\right)\right]\right\} & \text{for } \frac{L_c}{2} \leq x \leq \frac{L_c}{2} + \delta L_c, \\ -(\tilde{Q}_5/2l_0)\exp\left[l\left(\frac{L_c}{2} + \delta L_c - x\right)\right] & \text{for } x \geq \frac{L_c}{2} + \delta L_c \end{cases} \quad \text{(B.1b)}$$

clearly satisfy (2.7), since they also satisfy the boundary condition that Ψ' decreases monotonically with distance away from the frontal vortex, Ψ'_3 and Ψ'_5 may be referred to as the streamfunction fields induced by the edge waves $\tilde{Q}_3$ and $\tilde{Q}_5$, respectively. Before using (B.1) in (2.6), it is algebraically useful to note that as a consequence of common trigonometric relations, (5.1) and (5.2) may be rearranged to prove that,

$$\tilde{Q}_3 = \tilde{Q}_5\left[\cos(\Delta\chi) + \tan\left(l_0Y' + \mathcal{P}_3 + \Delta\chi\right)\sin(\Delta\chi)\right]\exp(\gamma_3 - \gamma_5), \quad \text{(B.2a)}$$

$$\tilde{Q}_5 = \tilde{Q}_3\left[\cos(\Delta\chi) - \tan\left(l_0Y' + \mathcal{P}_3\right)\sin(\Delta\chi)\right]\exp(\gamma_5 - \gamma_3). \quad \text{(B.2b)}$$

Transforming (B.1) into deforming geostrophic coordinates, (B.2) may be applied to prove that at transition region 3,

$$\frac{\partial\Psi'}{\partial Y'} = \frac{\tilde{Q}_3}{2}\left\{\left[1 + e^{-\dot{i}L}\cos(\Delta\chi)\exp(\gamma_5 - \gamma_3)\right]\tan\left(l_0Y' + \mathcal{P}_3\right) + \sin(\Delta\chi)\exp(\gamma_5 - \gamma_3)\right\} \quad \text{(B.3a)}$$

whilst at transition region 5

$$\frac{\partial\Psi'}{\partial Y'} = \frac{\tilde{Q}_5}{2}\left\{\left[1 + e^{-\dot{i}L}\cos(\Delta\chi)\exp(\gamma_3 - \gamma_5)\right]\tan\left(l_0Y' + \mathcal{P}_3\right) - \sin(\Delta\chi)\exp(\gamma_3 - \gamma_5)\right\}. \quad \text{(B.3b)}$$

The edge wave dynamics implied by (2.6) and (2.7) are now easily deduced.

Using (B.3a) and (5.1) in (2.6) and recalling that $\dot{L} = 2\mu$ leads to

$$\frac{\partial \gamma_3}{\partial T'} = (\delta\bar{\zeta}_n/2)\exp(-2\mu)\exp(\gamma_5 - \gamma_3), \tag{B.4a}$$

$$\frac{\partial \mathcal{P}_3}{\partial T'} = l_0\bar{v}_n - (\delta\bar{\zeta}_n/2)\left[1 + \exp(-2\mu)\exp(\gamma_5 - \gamma_3)\right], \tag{B.4b}$$

whilst using (B.3b) and (5.2) in (2.6) leads to

$$\frac{\partial \gamma_5}{\partial T'} = (\delta\bar{\zeta}_n/2)\exp(-2\mu)\exp(\gamma_3 - \gamma_5), \tag{B.4c}$$

$$\frac{\partial \mathcal{P}_3}{\partial T'} + \frac{\partial \Delta\chi}{\partial T'} = -l_0\bar{v}_n + (\delta\bar{\zeta}_n/2)\left[1 + \exp(-2\mu)\exp(\gamma_5 - \gamma_3)\right]. \tag{B.4d}$$

REFERENCES

Bishop, C.H., 1993b: On the behaviour of baroclinic waves undergoing horizontal deformation. Part 2: Error bound amplification and Rossby wave diagnostics. *Quart.J.R.Met.Soc.* 119, 241-269.

Bishop, C.H. and A.J. Thorpe, 1993: Frontal wave stability during moist deformation frontogenesis. Part 1. Linear wave dynamics. *J.Atmos.Sci.* (Submitted).

Bretherton, F.P., 1966. Baroclinic instability and the short wave cutoff in terms of potential vorticity. *Quart.J.R.Met.Soc.* 92,335-345.

Dritschel, D. G. 1988: The repeated filamentation of two-dimensional vorticity interfaces. *J. Fluid Mech.* 194, 511-547.

Dritschel, D. G., P.H. Haynes, M.N. Juckes, and T.G. Shepherd, 1991: The stability of a two-dimensional vorticity filament under uniform strain. *J. Fluid Mech.* 230, 647-665.

Farrell, B.F., 1984: Modal and non-modal baroclinic waves. *J.Atmos.Sci.*, 41:668-673.

Gall, R.L., R.T. Williams and T.L. Clark, 1987. On the minimum scale of fronts. *J. Atmos. Sci.*, 44, 2562-2574.

Garner, S.T., 1989. Fully Lagrangian numerical solutions of unbalanced

frontogenesis and frontal collapse. *J. Atmos. Sci.*, 46, 717-739.

Grabowski, W.W. and T.L. Clark, 1991. Cloud-environment interface instability: Rising thermal calculations in two spatial dimensions. *J.Atmos.Sci.*,48,527-546

Joly, A. and Thorpe,A.J. 1990: Frontal instability generated by tropospheric potential vorticity anomalies. *Quart.J.R.Met.Soc.*, 116: 528-560.

Joly, A. and A.J. Thorpe, 1991: The stability of time dependent flows: An application to fronts in developing baroclinic waves. *J.Atmos.Sci.*,48,163-182.

Nielson J.W. and R.M. Dole, 1991: A survey of extratropical cyclone characteristics during GALE. *Mon. Wea. Rev.* 120: 1156 - 1167.

Neiman P.J., M.A. Shapiro and L.S. Fedor, 1991: Synoptic and Mesoscale characteristics within an intense extratropical cyclone: ERICA IOP4, 4-5 January 1989. Preprints of First International Symposium on Winter Storms. pp 145-150. published by American Meteorological Society. pp 108-114.

Shapiro, M.A., T. Hampel, D. Rotzoll and F. Mosher, 1985: The frontal hydraulic head: A microscale (~1km) triggering mechanism for convective weather systems. *Mon. Wea. Rev.*, 113, 1166-1183.

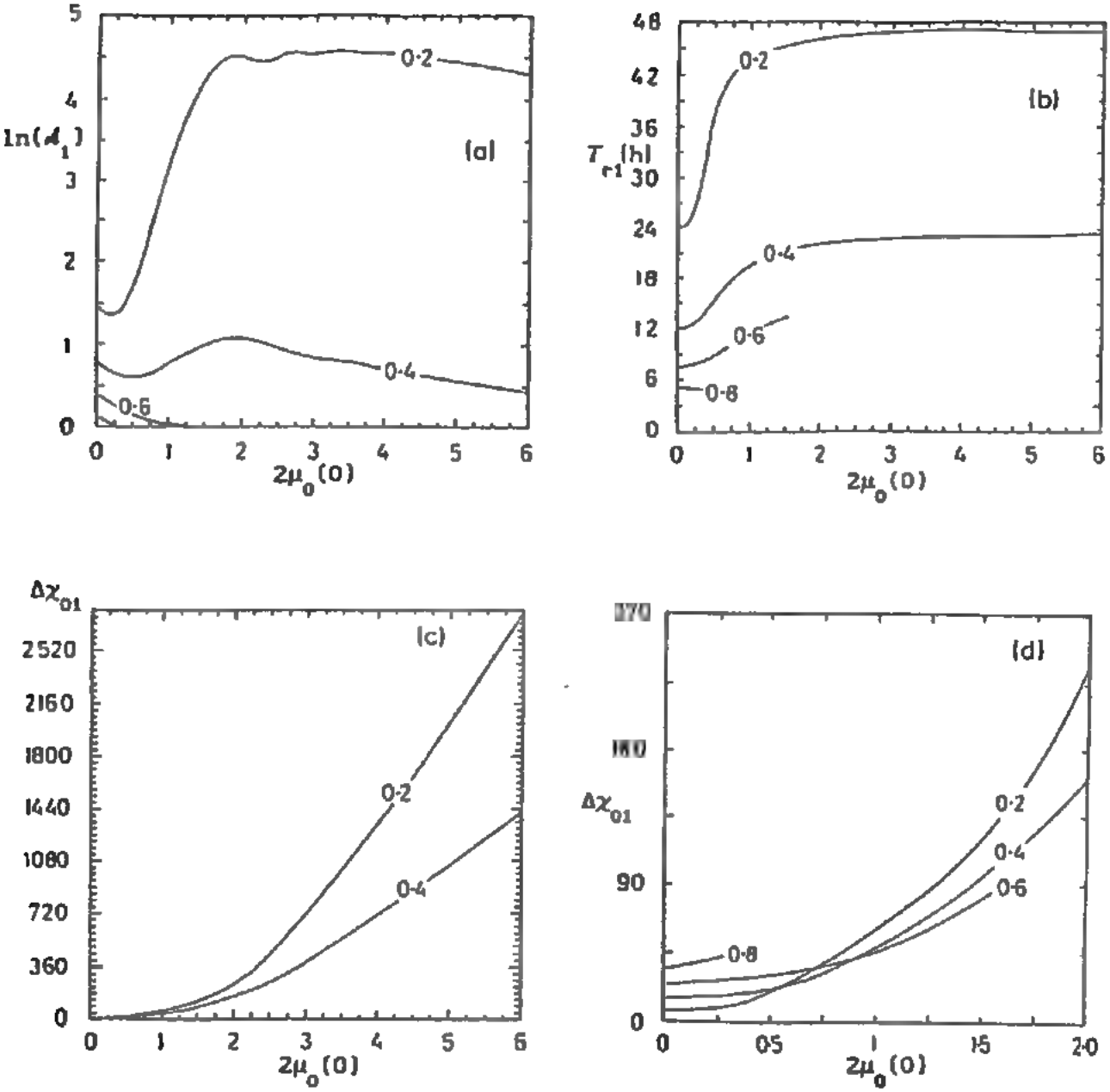

Fig.1 .

(a) Variation of $\ln(\mathcal{A}_1)$ with initial wavenumber, $2\mu_0(0)$, for a variety of strain rates, α. In this and subsequent diagrams line labels 0.2, 0.4, 0.6, 0.8 and 1.0 pertain to strain rates of $0.2\times10^{-5}s^{-1}$, $0.4\times10^{-5}s^{-1}$, etc.

(b) Time, T_{r1}, over which amplification $\mathcal{A}_1$ occurs as a function of $2\mu_0(0)$.

(c) The initial phase shift southward, $\Delta\chi_{01}$ (in degrees), of the eastern relative to the western wave required to produce the $\mathcal{A}_1$ amplification.

(d) Details of the phase changes shown in (c) for $0 \leq 2\mu_0(0) \leq 2$

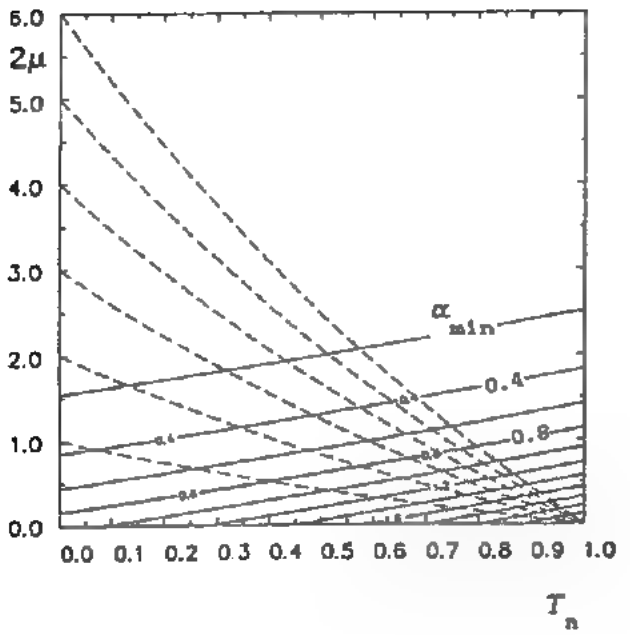

Fig. 2. Solid lines mark contours of the surface of minimum strain rate, $\alpha_{min}(T_n, 2\mu)$, required to totally prohibit growth; contour interval is $0.2\times10^{-5}s^{-1}$. Dashed lines show how, due to the evolving basic state, 2μ varies with T_n. For a given strain rate, α_g, and a given instantaneous non-dimensional wavenumber, $2\mu_g$, frontal wave steepening is only possible if $\alpha_g < \alpha_{min}$.

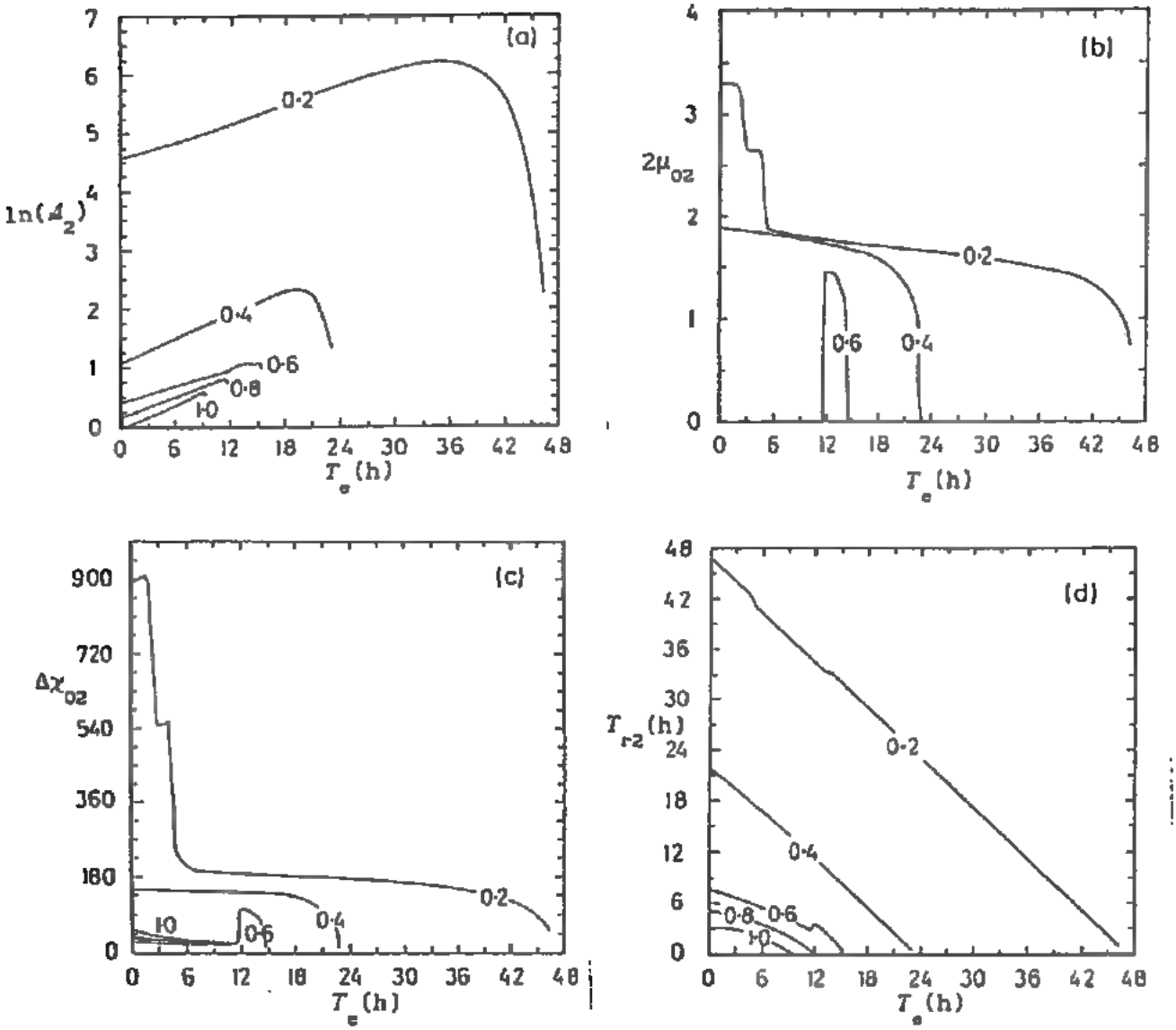

Fig. 3. The variations of $\ln(\mathcal{A}_2)$, $2\mu_{02}$, $\Delta\chi_{02}$ and T_{r2} with entry time T_e are shown in (a), (b), (c) and (d), respectively.

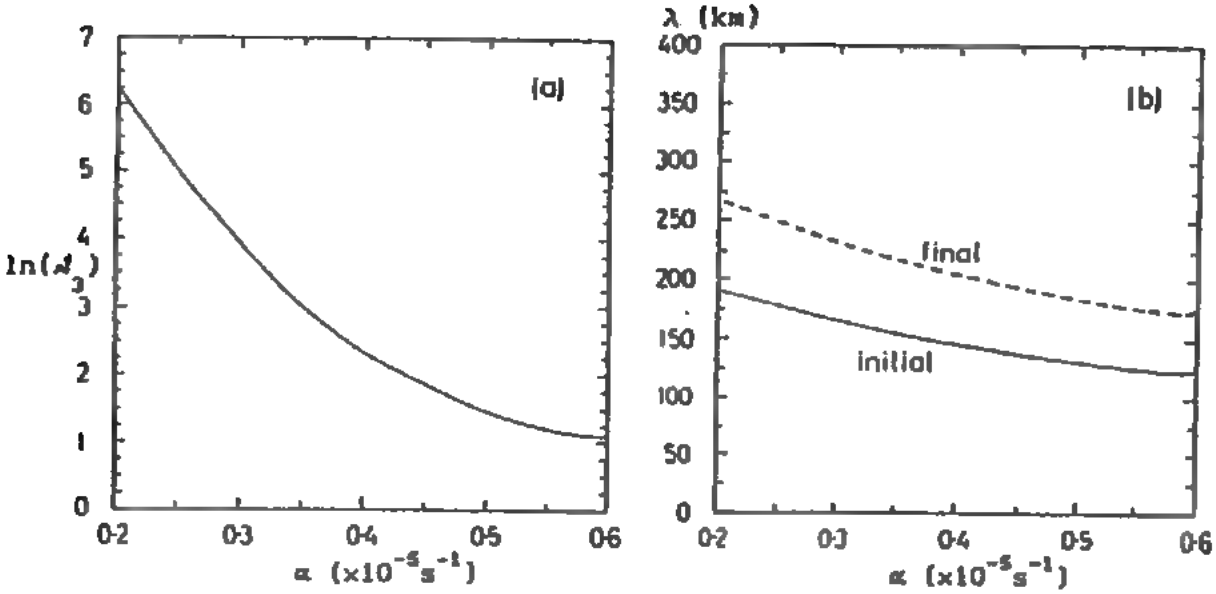

Fig. 4.

(a) $\ln(\mathcal{A}_3)$ as a function of the strain rate α

(b) The variation with α of the initial and final (dimensional) wavelengths of waves producing the $\mathcal{A}_3(\alpha)$ amplification are depicted by solid and dashed lines, respectively. These dimensional wavelengths were obtained by assuming the vortex strip to be 173 km wide at the time the vorticity equaled f.

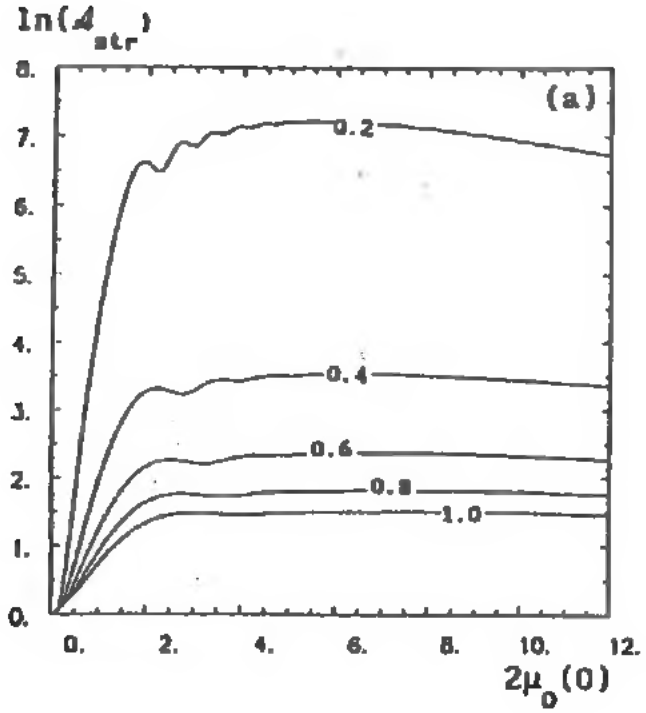

Fig. 5.

(a) The maximal streamfunction amplification versus non-dimensional wavenumber for for waves entering the frontal zone at $T_e = 0$ is shown for a range of strain rates.

CURRENT JCMM INTERNAL REPORTS

This series of JCMM Internal Reports, initiated in 1993, contains unpublished reports and also versions of articles submitted for publication. The complete set of Internal Reports is available from the National Meteorological Library on loan, if required.

1. **Research Strategy and Programme.**
   K A Browning et al
   January 1993

2. **The GEWEX Cloud System Study (GCSS).**
   GEWEX Cloud System Science Team
   January 1993

3. **Evolution of a mesoscale upper tropospheric vorticity maximum and comma cloud from a cloud-free two-dimensional potential vorticity anomaly.**
   K A Browning
   January 1993

4. **The Global Energy and Water Cycle**
   K A Browning
   July 1993

5. **Structure of a midlatitude cyclone before occlusion.**
   K A Browning and N Roberts
   July 1993

6. **Developments in Systems and Tools for Weather Forecasting.**
   K A Browning and G Szejwach
   July 1993

7. **Diagnostic study of a narrow cold frontal rainband and severe winds associated with a stratospheric intrusion.**
   K A Browning and R Reynolds
   August 1993

8. **Survey of perceived priority issues in the parametrizations of cloud-related processes in GCMs.**
   K A Browning
   September 1993

9. **The Effect of Rain on Longwave Radiation.**
   I Dharssi
   September 1993

10. **Cloud Microphysical Processes - A Description of the Parametrization used in the Large Eddy Model.**
    H Swann
    October 1993

11. **An Appreciation of the Meteorological Research of Ernst Kleinschmidt.**
A J Thorpe
May 1992

12. **Potential Vorticity of Flow Along the Alps.**
A J Thorpe, H Volkert and Dietrich Heimann
August 1992

13. **The Representation of Fronts.**
A J Thorpe
January 1993

14. **A Parametrization Scheme for Symmetric Instability: Tests for an Idealised Flow.**
C S Chan and A J Thorpe
February 1993

15. **The Fronts 92 Experiment: a Quicklook Atlas.**
Edited by T D Hewson
November 1993

16. **Frontal wave stability during moist deformation frontogenesis.**
Part 1. Linear wave dynamics.
C H Bishop and A J Thorpe
May 1993

17. **Frontal wave stability during moist deformation frontogenesis.**
Part 2. The suppression of non-linear wave development.
C H Bishop and A J Thorpe
May 1993

Met Office Joint Centre for Mesoscale Meteorology Department of Meteorology
University of Reading PO Box 243 Reading RG6 6BB United Kingdom
Tel: +44 (0)118 931 8425 Fax: +44 (0)118 931 8791
www.metoffice.com